Computational modeling of deformation mechanisms and failure in thermoplastic multilayer composites

Th. Seelig

Computational modeling of deformation mechanisms and failure in thermoplastic multilayer composites

Th. Seelig

PII: S0266-3538(07)00297-7
DOI: 10.1016/j.compscitech.2007.07.017
Reference: CSTE 3788

To appear in: *Composites Science and Technology*

Received Date: 3 April 2007
Revised Date: 27 June 2007
Accepted Date: 30 July 2007

Please cite this article as: Seelig, Th., Computational modeling of deformation mechanisms and failure in thermoplastic multilayer composites, *Composites Science and Technology* (2007), doi: 10.1016/j.compscitech.2007.07.017

Computational modeling of deformation mechanisms and failure in thermoplastic multilayer composites

Th. Seelig*

Fraunhofer-Institute for Mechanics of Materials, Woehlerstrasse 11, 79108 Freiburg, Germany

Abstract

The deformation and failure behavior of composites consisting of multiple alternating layers of a brittle and a ductile amorphous thermoplastic polymer is controlled by the interaction between crazing and shear banding and displays a brittle-to-ductile transition depending on the composition. In order to gain a better understanding of these interrelations in PC/SAN multilayer composites numerical simulations are performed and compared with experimental observations. The set-up of the computational problem utilizes constitutive models for the large strain viscoplastic behavior of glassy polymers as well as a cohesive surface methodology describing the localized formation, growth and breakdown of crazes. The simulations well reproduce the strong dependence of the mode of failure on the relative layer thickness and help to explain how the latter determines whether the composites display a ductile overall response or undergo localized brittle failure by the coalescence of microcracks.

KEYWORDS

A. Layered structures; A. Polymers; B. Plastic deformation; Crazing; C. Finite element analysis (FEA)

*Tel.:+49-761-5142-274; Fax.:+49-761-5142-110; E-mail: see@iwm.fhg.de (Th. Seelig)

1 Introduction

Under tensile loading at room temperature, the deformation behavior of amorphous thermoplastic polymers differs significantly and ranges from the high ductility and ability to undergo large inelastic strains (e.g. cold drawing) of polycarbonate (PC) to the brittleness of polystyrene (PS) or styrene-acrylonitrile (SAN) which typically fail at a few percent of strain (e.g. Kinloch and Young, 1983). Brittle failure in these materials takes place by crazing, i.e. the formation of highly localized narrow zones, normal to the principal tensile stress, in which the polymer material is drawn into numerous thin fibrils. Though the fibrillated craze matter is still capable of carrying stress, rupture of the fibrils (typically at a length of the order of a micron) turns a craze into a crack and gives rise to brittle failure with a low amount of overall energy dissipation due to the localized nature of the crazes. The tendency of the majority of glassy polymers to undergo crazing limits their applicability for technical products and various strategies to control this damage mechanism have been developed; see e.g. (Bucknall, 1977) and (Martuscelli, 1996).

A relatively recent method of producing materials with a heterogeneous microstructure which hinders the unlimited growth of crazes is multilayer coextrusion of two different glassy polymers. The mechanical performance of such materials with a well defined composition of multiple microlayers of PC and SAN has been investigated experimentally by Gregory et al. (1987), Sung et al. (1994), Kerns et al. (2000); see also (Im et al., 1991). For tensile loading parallel to the layers, it was found that the overall elastic stiffness of these composites clearly (and as expected) follows a "rule of mixtures" but the nonlinear deformation and especially the fracture behavior does not. Under loading beyond the linear elastic regime several isolated crazes form in the brittle SAN, which extend over the whole width of the SAN layers and arrest at the SAN/PC interfaces. Starting from the craze tips at the interfaces, shear bands then initiate in the neighboring ductile PC layers. Figure 1 shows micrographs of these experiments on SAN-rich composites (a) and PC-rich composites (b) and (c). The thickness of the PC and SAN layers is approximately $9\,\mu$m and $22\,\mu$m in Fig. 1a while it is approximately $44\,\mu$m and $13\,\mu$m in Fig. 1b and c. For both compositions a network of crazes and shear bands, the latter oriented at about 45°, has formed throughout the material (Figs. 1a and b). However, while SAN-rich composites fail in a brittle manner at a few percent overall strain (fracture surface visible at bottom of Fig. 1a) PC-rich composites display a ductile overall behavior with a strain at fracture of up to about 80%. In this case the crazes open up to holes, typically arranged in a diagonal pattern, and the intermediate PC layers undergo large plastic strains (Fig. 1c). Ultimate specimen fracture then occurs when the PC layers start to fail and holes

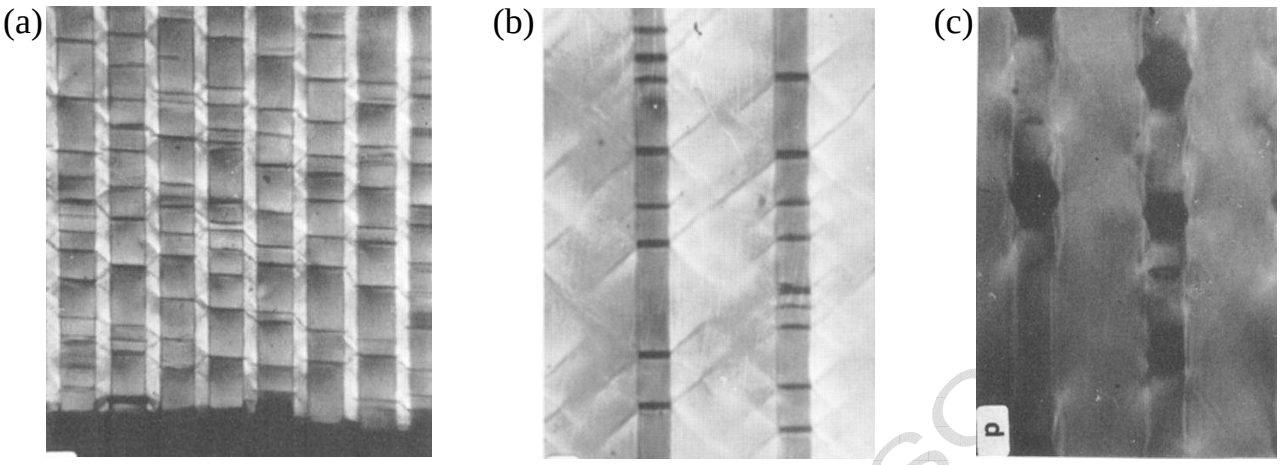

Figure 1: PC/SAN multilayer composites under tensile load showing crazing in SAN and shear banding in PC; from (Gregory et al., 1987) with permission.

coalesce. As can be seen from the micrographs in Fig. 1 and is reported by the authors of the experimental work, neither crazing in PC nor interface delamination between the two phases takes place. The general conclusion drawn from the experimental investigation is that for a sufficient amount of PC (i.e. relative layer thickness) the interaction between crazes and shear bands in these composites effectively hampers the formation and propagation of a macroscopic crack. The aim of the present work is to explore, by means of numerical simulations, the brittle-to-ductile transition in the overall response of PC/SAN multilayer composites controlled by their composition and to gain a better understanding of the beneficial role of the underlying micromechanisms.

Modeling the complex micro- and macromechanical behavior of thermoplastic multilayer composites requires a proper description of their individual constituents. Constitutive models for glassy polymers that account for their characteristic rate- and temperature dependent behavior, comprising softening and rehardening, as it results from the macromolecular structure of these materials are now available and have been successfully applied in various numerical analyses (e.g. Boyce et al., 1988; Haward and Young, 1997; Tomita 2000; Meijer and Govaert, 2003). In particular, the characteristic feature of localization of deformation in shear bands, promoted by the intrinsic softening, has been investigated in detail by Van der Giessen (1997), Pijnenburg et al. (1999) and Danielsson et al. (2002) with application to plastic zone formation at notches or the spreading of plasticity in the glassy matrix of rubber-toughened polymers. Shear bands also play a crucial role in the deformation of multilayer composites focused on in

the present work. The second typical deformation (or damage) mechanism in glassy polymers, crazing, has likewise been studied numerically by several authors (Tijssens et al., 2000; Estevez et al. 2000; Socrate et al., 2001; Estevez and Van der Giessen, 2005); yet, despite the large number of experimental investigations, see e.g. (Michler, 1992; Narisawa and Yee, 1993), the understanding and data basis is much less clear than with regard to the bulk deformation. Computational modeling of multilayer composites of two glassy polymers where both mechanisms, shear banding and crazing, coexist, as attempted in the present work, may therefore not only help to better understand this class of composites but may also yield information about the crazing process itself and related physical quantities.

In Sect. 2 we start out by presenting the constitutive models utilized in the description of the individual phases of PC/SAN multilayer composites. The large strain viscoplastic behavior of PC is captured by the model discussed in Sect. 2.1, and a cohesive surface methodology, adopted to describe the initiation, growth and breakdown (i.e. microcrack formation) of crazes, is presented in Sect. 2.2. In Sect. 3 the set-up of the boundary value problem is explained. Numerical results for two model composites, one PC-rich and the other SAN-rich, are presented in Sect. 4. They are analyzed with respect to the influence of composition (in terms of relative layer thickness) on the local interaction of crazes (or cracks) and shear bands as well as on the overall response of the composites. Besides the comparison with experimental findings, the simulations provide additional information not accessible by experiments such as the amount of energy dissipated by the different micromechanisms in the course of overall deformation and failure.

2 Constitutive models

2.1 Deformation behavior of glassy polymers

In the absence of crazing all glassy thermoplastic polymers display a common characteristic deformation behavior which results from their amorphous molecular structure. It consists of a small elastic deformation regime, a pronounced yield point followed by intrinsic softening, rate-dependent flow, and progressive rehardening due to molecular alignment at large stretches (e.g. Haward and Young, 1997). A model that well captures these features has been developed by Boyce et al. (1988) and is employed here in the slightly modified version given in (Wu and Van der Giessen, 1996); its typical response is shown in Fig. 2.

The theory makes use of the standard additive decomposition of the rate of deformation

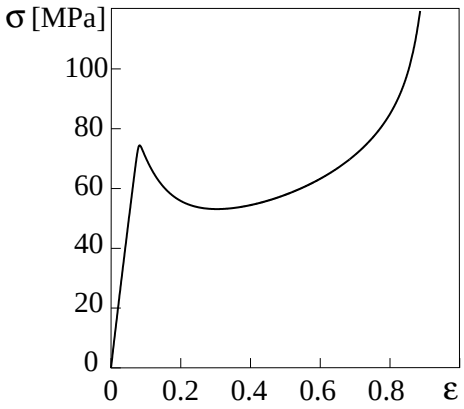

Figure 2: Plane strain tension response of PC in terms of true stress vs. logarithmic strain at constant strain rate $\dot{\varepsilon} = 0.01\,\mathrm{sec}^{-1}$ and room temperature, computed from data in Table 1.

tensor into its elastic and plastic parts: $\boldsymbol{D} = \boldsymbol{D}^{\mathrm{e}} + \boldsymbol{D}^{\mathrm{p}}$. Visco-elastic effects prior to yield are neglected in the present study. The small strain elastic response is governed by Hooke's law written in (hypoelastic) rate form as

$$\boldsymbol{D}^{\mathrm{e}} = \boldsymbol{\mathcal{L}}^{-1}\,\overset{\nabla}{\boldsymbol{\sigma}} \tag{1}$$

where $\overset{\nabla}{\boldsymbol{\sigma}}$ is the Jaumann rate of the Cauchy stress and $\boldsymbol{\mathcal{L}}$ is the standard fourth-order isotropic elasticity tensor. The isochoric visco-plastic strain rate

$$\boldsymbol{D}^{\mathrm{p}} = \frac{\dot{\gamma}^{\mathrm{p}}}{\sqrt{2}\tau}\bar{\boldsymbol{\sigma}}' \tag{2}$$

is specified in terms of the equivalent plastic shear strain rate $\dot{\gamma}^{\mathrm{p}} = \sqrt{\boldsymbol{D}^{\mathrm{p}} \cdot \boldsymbol{D}^{\mathrm{p}}}$ and the deviatoric driving stress $\bar{\boldsymbol{\sigma}}'$ normalized by the equivalent driving shear stress $\tau = \sqrt{\frac{1}{2}\bar{\boldsymbol{\sigma}}' \cdot \bar{\boldsymbol{\sigma}}'}$. The latter serves to determine $\dot{\gamma}^{\mathrm{p}}$ via the visco-plastic constitutive equation

$$\dot{\gamma}^{\mathrm{p}} = \dot{\gamma}_0 \exp\left[-\frac{A\tilde{s}}{\theta}\left(1 - \left(\frac{\tau}{\tilde{s}}\right)^{5/6}\right)\right] \tag{3}$$

where $\dot{\gamma}_0$ and A are material parameters, and θ is the absolute temperature which is taken constant in the present study. The shear resistance $\tilde{s}$ in (3) evolves with the plastic strain according to

$$\tilde{s}(\gamma^{\mathrm{p}}) = s_s + (s_0 - s_s)\exp\left(-h\gamma^{\mathrm{p}}/s_s\right) + \alpha p \tag{4}$$

from the initial, athermal yield strength s_0 to a saturation value s_s in order to phenomenologically describe the intrinsic softening of the glassy polymer (Fig. 2); see e.g. (Boyce et al.,

1988) for details on the molecular background of this behavior. Furthermore, (4) incorporates the well-known dependence of yield in polymers on the pressure $p = -\frac{1}{3}\mathrm{tr}\boldsymbol{\sigma}$ via the constant pre-factor α. This pressure dependence is due to a changing molecular mobility and is not associated with plastic dilatancy of the bulk material, as $\mathrm{tr}\boldsymbol{D}^{\mathrm{p}} = 0$ according to (2).

The progressive hardening after yield due to stretching and alignment of the molecular network is described by the back stress tensor $\boldsymbol{b}$ incorporated in the driving stress tensor $\bar{\boldsymbol{\sigma}}' = \boldsymbol{\sigma}' - \boldsymbol{b}$. Drawing on the analogy with cross-linked rubber (Arruda and Boyce, 1993), the principal components of the back stress tensor are specified in terms of principal stretches. The back stress model involves two additional material parameters: the initial hardening modulus C_R and the limit stretch of the molecular chains $\lambda_{\max}$ at which the network responds with an infinite stiffness and no further yielding is possible. Full details of the constitutive model and the employed explicit numerical integration scheme may be found in (Wu and Van der Giessen, 1996). The set of material parameters for PC is listed in Table 1.

Table 1: Material parameters used for PC at room temperature in the present work, adopted from (Boyce et al., 1988).

	E [MPa]	ν	s_0 [MPa]	s_s/s_0	As_0/θ	h/s_0	α	$\lambda_{\max}$	C^R/s_0	$\dot{\gamma}_0$ [sec^{-1}]
PC	1500	0.3	97	0.79	79.2	5.15	0.08	2.5	0.059	$2{\cdot}10^{15}$

An analogous set of material parameters for SAN, needed to describe its large strain viscoplastic behavior under compression or shear, is also available in the literature (Pijnenburg et al., 1999). In the present context, however, where only tensile loading is considered and SAN displays crazing prior to any plasticity, its bulk deformation is sufficiently described as linear elastic with Young's modulus $E = 3000\,\mathrm{MPa}$ and Poisson's ratio $\nu = 0.38$. It should be mentioned that the values for the Young's moduli of PC and SAN given above are taken somewhat smaller than those typically found in the literature in order to capture the effect of small strain viscoelasticity not explicitly accounted for in the constitutive model.

2.2 Cohesive surface modeling of crazing and failure

Failure of neat glassy polymers typically proceeds by the formation and propagation of crazes, i.e. highly localized crack-like zones oriented normal to the maximum principal tensile stress. Crazes consist of numerous thin fibrils (of a few nanometers thickness) of stretched molecular chains which are drawn from the bulk material in a rate-dependent process (e.g. Narisawa and

Yee, 1993; Haward and Young, 1997; Estevez et al., 2000, 2005). The fibrils connect the two craze-bulk interfaces and are able to transfer stress until they rupture and a craze locally turns into a crack, typically at a critical craze width (depending on the material) of the order of a micron or below. Representing the effect of stress-carrying fibrils between the separating craze-bulk interfaces in a "smeared" sense by a viscoplastic traction-separation law, Tijssens et al. (2000) have developed a cohesive surface model for crazing. It recognizes the three distinct stages of *craze initiation*, rate-dependent *craze widening* and *craze breakdown*. In a somewhat modified form this model is also employed in the present work in order to describe crazing and fracture in PC/SAN multilayer composites. The incorporation into a finite element discretization of the bulk material proceeds by the introduction of special cohesive elements characterized by a relation between the traction vector $\boldsymbol{T}$ and the separation $\boldsymbol{\Delta}$ of the two craze-bulk interfaces. Prior to craze widening the cohesive elements have zero thickness, i.e. pairs of nodes are located at identical positions (Fig. 3a). Owing to the fibrillar structure of the craze matter the cohesive traction vector is taken collinear to the separation, i.e. $\boldsymbol{T} = T\,\dfrac{\boldsymbol{\Delta}}{\Delta}$ with $\Delta = \sqrt{\boldsymbol{\Delta}\cdot\boldsymbol{\Delta}}$.

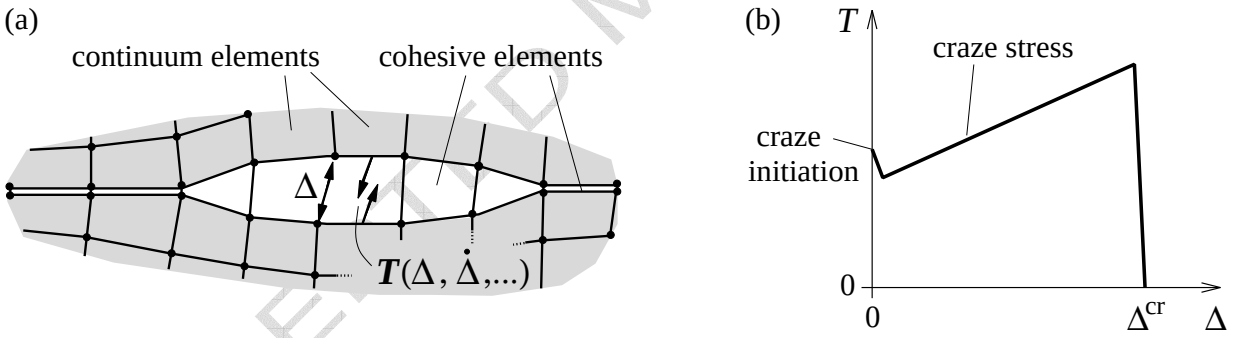

Figure 3: (a) Cohesive zone model of a craze, (b) traction-separation law for crazing at constant separation rate.

Among the various criteria for craze initiation in glassy polymers discussed in the literature (e.g. Kinloch and Young, 1983; Michler, 1992; Narisawa and Yee, 1993) those based on a critical stress state appear most suitable in the present context. Recent experiments by Saad-Gouider et al. (2006) indicate that in brittle polymers such as PMMA craze initiation is controlled by a critical value of the maximum principal tensile stress, whereas for ductile polymers (e.g. PC where crazing is preceded by localized plastic deformation) a critical hydrostatic stress is appropriate. Craze initiation in SAN, which is quite similar to PMMA in terms of brittleness and molecular charactersitics relevant for crazing (e.g. entanglement density), hence is likely to be

also governed by a principal tensile stress criterion. Therefore, we assume here that crazing initiates locally on a cohesive surface in SAN when the critical tensile stress $T = \sigma_c^{init}$ (at this stage normal to the still closed cohesive surface!) is reached.

The relation between the cohesive traction T and the separation Δ of the craze-bulk interfaces is written in the following elastic visco-plastic rate form (Tijssens et al., 2000)

$$\dot{T} = k\left(\dot{\Delta} - \dot{\Delta}_c\right) \ . \tag{5}$$

Prior to craze initiation the visco-plastic craze widening rate $\dot{\Delta}_c$ vanishes and the elastic stiffness k is a large, purely artificial 'penalty' parameter. After initiation k reflects the instantaneous elastic stiffness of the craze matter. Craze widening upon initiation is described by the visco-plastic relation

$$\dot{\Delta}_c = \dot{\Delta}_0 \exp\left[\frac{A_c}{\theta}\left(T - \sigma_c\right)\right] \tag{6}$$

where $\dot{\Delta}_0$ and A_c are material parameters, θ is the (here constant) absolute temperature and σ_c denotes the craze widening resistance (Tijssens et al., 2000). While the latter was taken constant in the numerical studies by Tijssens et al. (2000) and Estevez et al. (2000, 2005) there is strong evidence – from experiments as well as theoretical models (Gregory et al., 1987; Sung et al., 1994; Basu et al., 2005) – that the craze stress vs. craze widening displays a hardening-like behavior. Here we assume a linear evolution of the craze widening resistance with the inelastic separation

$$\sigma_c(\Delta_c) = \sigma_c^{init}\left(1 + h_c\,\frac{\Delta_c}{\Delta_c^{cr}}\right) \qquad \text{for} \qquad \Delta_c \in [0, \Delta_c^{cr}] \tag{7}$$

where σ_c^{init} denotes the craze widening resistance at craze initiation and h_c is a constant; the calibration of the involved parameters is discussed in the following paragraph. Evaluated at a constant separation rate the traction-separation law displays the behavior sketched in Fig. 3b. The indicated eventual stress drop right after initiation results from the difference between the rate parameter $\dot{\Delta}_0$ (or $\dot{\Delta}_c$ at $T = \sigma_c^{init}$) and the actual separation rate $\dot{\Delta}$.

Values for the material parameters involved in the cohesive zone model for crazing are fairly unclear, they are hardly accessible to direct measurements, and they result from complex processes on the molecular level such as disentanglement and chain-scission taking place at the craze-bulk interface (e.g. Haward and Young, 1997; Estevez et al., 2000, 2005). In order to calibrate the model from a macroscopic point of view we make use of experimental results by Gregory et al. (1987) and Sung et al. (1994). In tensile tests on neat SAN they observed the first appearance of crazing at about 1-2 % strain and a stress level of 40-50 MPa while ultimate brittle failure took place at 3-4 % strain and around 70-80 MPa. This increase of the overall

stress in the course of continued straining accompanied by crazing motivates the assumption of a hardening-like traction-separation law. The underlying increase of the craze widening resistance is understood to result from stretching of the molecular chains in the craze fibrils (e.g. Lauterwasser and Kramer, 1979). This view is also supported by detailed micromechanical analyses of the fibril drawing process by Basu et al. (2005) who found that the craze stress prior to failure may become as high as the bulk yield stress ($\approx 100\,\mathrm{MPa}$). Based on the experimental value of $\sigma_c^{init} \approx 40\,\mathrm{MPa}$ this provides an estimate of $h_c \approx 1.5$ in (7). The parameter Δ_c^{cr} which denotes the critical craze width (separation) at which a craze looses its stress-carrying capacity is determined from the following considerations: The total tensile strain of SAN at maximum load, i.e. right before brittle failure, involves the elastic strain of the intact bulk material plus an extra strain due to widening of the localized crazes

$$\varepsilon_f = \frac{\sigma_f}{E} + \frac{\Delta_c^{cr}}{l_c} \tag{8}$$

where ε_f and σ_f are the failure strain and stress and l_c denotes the average spacing of the crazes. With the values reported by Gregory et al. (1987) of $\varepsilon_f \approx 0.04$ and $\sigma_f \approx 75\,\mathrm{MPa}$ this yields $\Delta_c^{cr}/l_c \approx 0.015$. From the micrographs in Fig. 1a and b the average spacing l_c between crazes in the SAN layers is about $20\,\mu$m for both compositions. That mean that the critical craze width Δ_c^{cr} at breakdown has to be about $0.3\,\mu$m which is in line with values reported in the literature (e.g. Michler, 1992). The remaining, less significant parameters are adopted from (Estevez et al., 2000) and the values used in the present work are summarized in Table 2.

Table 2: Material parameters used in the cohesive surface model for crazing in SAN at room temperature in the present work.

σ_c^{init} [MPa]	Δ_c^{cr} [μm]	h_c	$A_c\sigma_c^{init}/\theta$	$\dot{\Delta}_0/\Delta_c^{cr}$ [sec^{-1}]	$k\Delta_c^{cr}$ [MPa]
40	0.3	1.5	18	1.6×10^4	6×10^3

In the tensile tests reported on PC/SAN multilayer composites failure of PC did not proceed by crazing but by brittle rupture after it had undergone large plastic stretching (Gregory et al., 1987). Beyond a stretch of about 2, i.e. 80% of the limit stretch $\lambda_{\max}$ (Table 1), the stress in PC rapidly rises because the molecular chains are aligned and no further plastic deformation is possible (see also Fig. 2). A critical tensile stress (normal to the cohesive surface) of 150 MPa according to Seitz (1993) is taken here as a criterion for failure of PC provided that the plastic stretch (computed from neighboring continuum elements) is larger than 2. Analogous to crazing

in SAN this criterion is evaluated on the cohesive surfaces, and likewise craze breakdown in SAN, brittle rupture (at zero length of decohesion) of the plastically stretched PC is treated numerically be releasing the cohesive traction to zero in a small number of time steps. For details on the numerical treatment of the rate-dependent cohesive surface model the reader is referred to (Tijssens et al., 2000) or (Estevez et al., 2000).

3 Modeling PC/SAN multilayer composites

In order to investigate the interaction of crazing and shear banding in PC/SAN multilayer composites numerically we consider a sample of such a material as illustrated in Fig. 4a. Plane strain conditions are assumed and the two-dimensional model problem consists of alternating layers of PC and SAN described by the constitutive models presented in Sect. 2.1. Overall loading parallel to the layers is imposed in terms of a prescribed velocity $\dot{u}$ on the upper boundary so that the sample of height h is subjected to a constant macroscopic strain rate $\dot{\bar{\varepsilon}} = \dot{u}/h$. Shear stresses on all boundaries are zero. To mimic a larger sample than actually modeled symmetry boundary conditions with vanishing macroscopic normal stresses are imposed on the lateral boundaries. Along with the finite element discretization of the whole sample several cohesive surfaces are introduced normal to the overall loading direction (Fig. 4a). The cohesive surfaces are locations of potential failure and their response is described by the cohesive model for crazing inside the SAN layers while inside the PC layers they are governed by the criterion for rupture (Sect. 2.2). The spacing between the cohesive surfaces is constant and corresponds to the typical average spacing between crazes observed in real multilayer composites (see Fig. 1). As already mentioned in the Introduction, debonding along the PC/SAN interfaces did not take place in the experiments; hence, it is also not considered in the computational model.

Once a craze in the SAN initiates and widens, the bulk continuum elements adjacent to the respective cohesive surface separate whereas the neighboring PC remains intact. To account for this particular kinematics at a PC/SAN interface, PC and SAN continuum elements adjacent to a junction point between a cohesive surface and an interface are allowed to slide relative to each other (accomplished by one cohesive element along the interface above and below the craze zone) as illustrated by the succession of snap-shots in Fig. 4b-e. In the last of these snap-shots (Fig. 4e), taken from one of the simulations presented in Sect. 4, the PC has already reached the state where failure sets on along the cohesive surface.

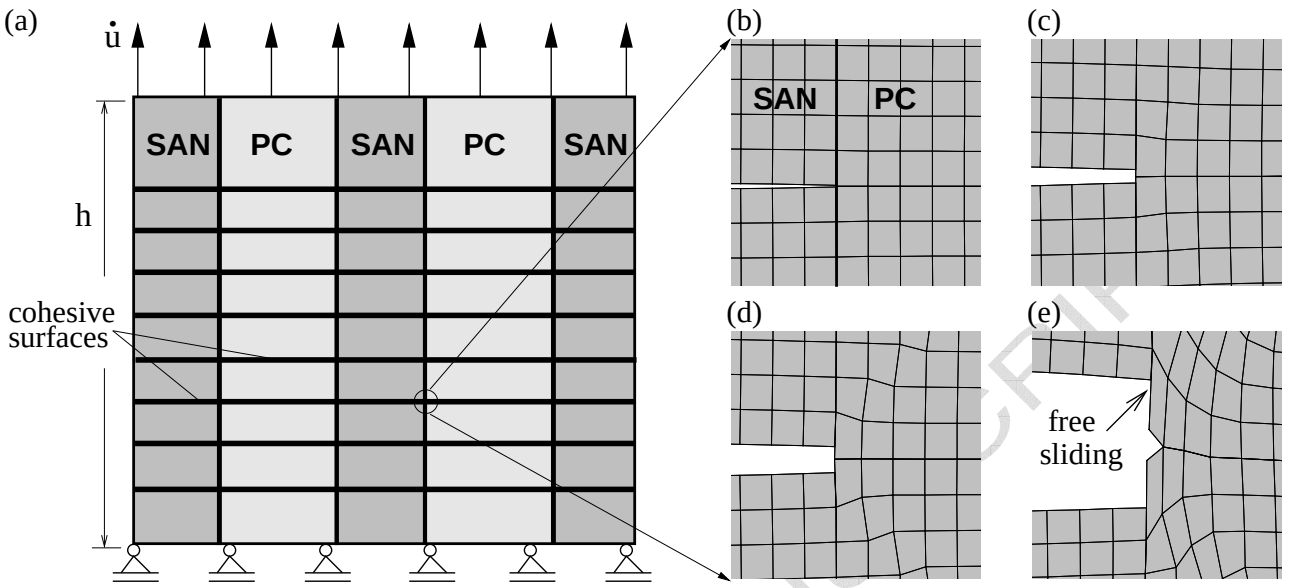

Figure 4: (a) Modeling PC/SAN multilayer composites with cohesive surfaces for potential failure, (b)-(e) details of the cohesive element modeling of crazing and crack opening at interface.

4 Numerical results

In the following we consider two model composites, one PC-rich with a relative layer thickness (volume fraction) of PC/SAN = 3/1, and the other SAN-rich with PC/SAN = 1/3. These compositions correspond to those investigated experimentally by Gregory et al. (1987); see Fig. 1. An overall strain rate of $\dot{\bar{\varepsilon}} = 1\,\mathrm{sec}^{-1}$ is prescribed which is in the range of loading rates in the experiments.

Inelastic deformation in real PC/SAN multilayer composites starts by the formation of several isolated crazes in the SAN from statistically distributed initial defects. From the experiments discussed in the Introduction it could not be detected when in the course of loading, prior to or accompanied by shear banding in the PC, crazes lose their stress-carrying capacity and become microcracks. The purpose of the present study is to gain some deeper understanding of the interaction of crazing and shear banding. We therefore first ignore the statistical nature of multiple initial defects and analyze in Sect. 4.1 the idealized situation where crazing is enforced to start from one particular cohesive surface by choosing for it a somewhat lower craze initiation stress (10 % below σ_c^{init} from Table 2) than for the other (all equal) cohesive surfaces. The more realistic case of several distributed imperfections is considered in Sect. 4.2.

4.1 Failure initiation from a single craze

Figure 5 shows contours of accumulated plastic strain in the PC-rich composite at successive levels of overall strain. The sample of material consists of one PC layer in between two half layers of SAN and is subjected to tensile loading parallel to the layers. At the instant shown in Fig. 5a a pair of shear bands has formed in the PC, starting from the single initially weaker craze (in the left SAN layer) which has opened to a much larger extent than the other crazes. In fact, as can be seen from the stress drop in the overall response depicted in Fig. 6, this particular craze has already broken down and become a crack. As will be discussed below, the shear band kinematics induces a stress concentration in the right SAN layer which, at the subsequent instant shown in Fig. 5b, leads to the opening of two further crazes/cracks. The latter then act as initiation sites for new shear bands which spread back to the left SAN layer where they enforce widening of additional crazes (Fig. 5c). The spacing of the resulting separation zones in a SAN layer is about twice the thickness of the PC layer because of the 45° orientation of the shear bands. At continued overall deformation the shear bands broaden and the cracks in the SAN open up to holes (Fig. 5c) while the overall stress remains approximately constant (Fig. 6).

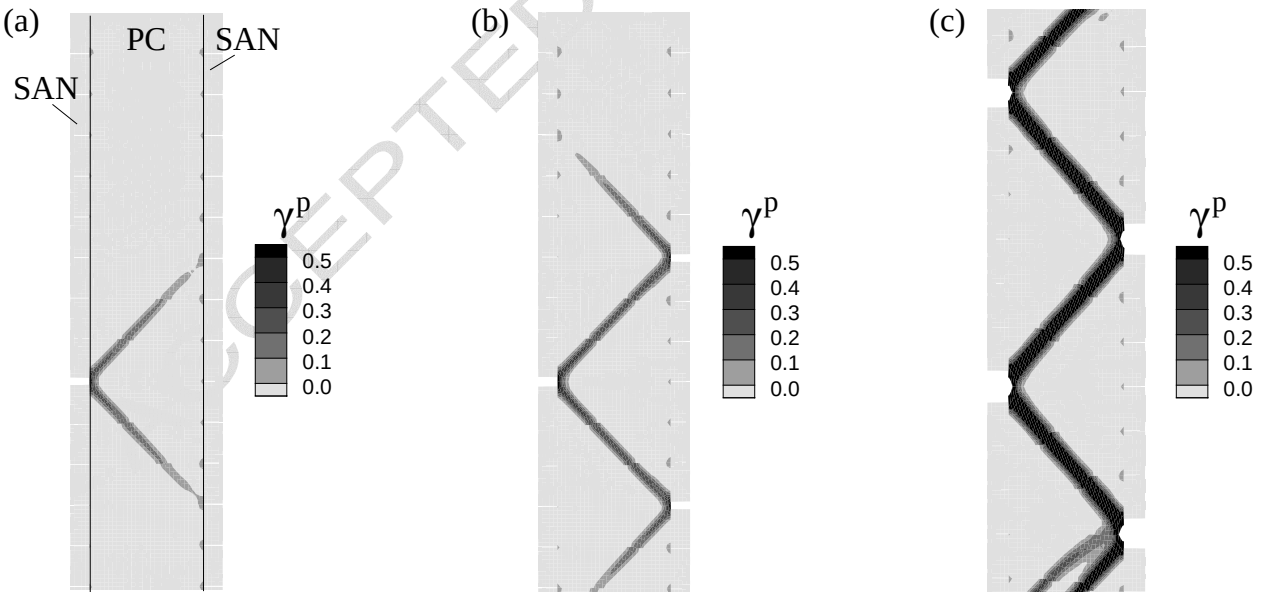

Figure 5: Contours of plastic strain γ^p in PC/SAN(3/1) microlayer composite at overall strain (a) $\bar{\varepsilon} = 0.052$, (b) $\bar{\varepsilon} = 0.056$, (c) $\bar{\varepsilon} = 0.14$.

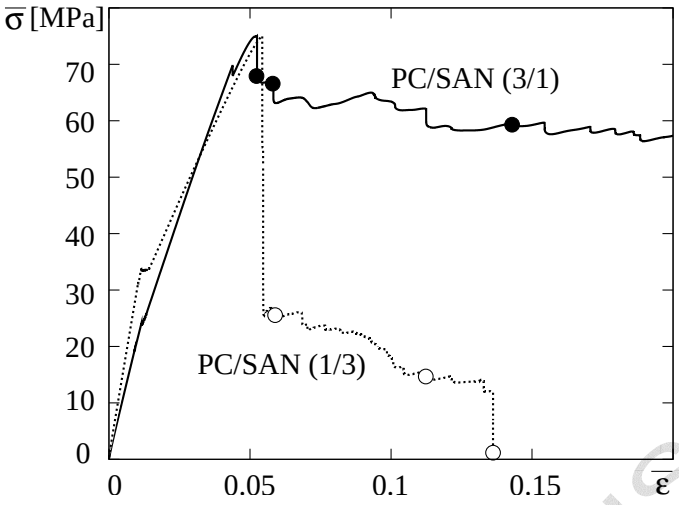

Figure 6: Macroscopic response of PC-rich and SAN-rich composites, symbols indicate instants referring to contour plots in Fig. 5 (•) and Fig. 7 (○), respectively.

The picture changes completely when the SAN-rich composite is considered (Fig. 7), again with one cohesive surface in the left SAN layer chosen somewhat weaker than the others. Because of the low distance between the SAN layers, the stress concentration caused by craze widening on the first cohesive surface promotes the initiation of further crazes in its vicinity. Craze breakdown on the weak cohesive surface entails immediate craze breakdown in the neighboring SAN layer as indicated by the dramatic stress drop visible in Fig. 6. The two resulting microcracks are visible in Fig. 7a and are both origins of separate pairs of shear bands. At continued overall straining (Fig. 7b) the region of plastic deformation does not spread in the composite – in contrast to the situation in Fig. 5 – and in this confined region plastic strains increase until rupture of the PC takes place and microcracks coalesce (Fig. 7c).

The overall response of both composites is depicted in Fig. 6 and differs fundamentally. While the PC-rich material displays a ductile behavior at a relatively high stress level, the SAN-rich composite fails in a brittle manner. Though the model considered so far is strongly simplified in terms of the number of layers and imperfections, the overall response of the different composites is in good qualitative agreement with experimental findings (Gregory et al., 1987). The final stable regime during fracture of the SAN-rich composite (see Fig. 6) is an artifact of the numerical crack path being restricted to the cohesive surfaces which do not allow the two early formed microcracks to directly link up.

The significantly different behavior of PC-rich and SAN-rich composites, i.e. the strong

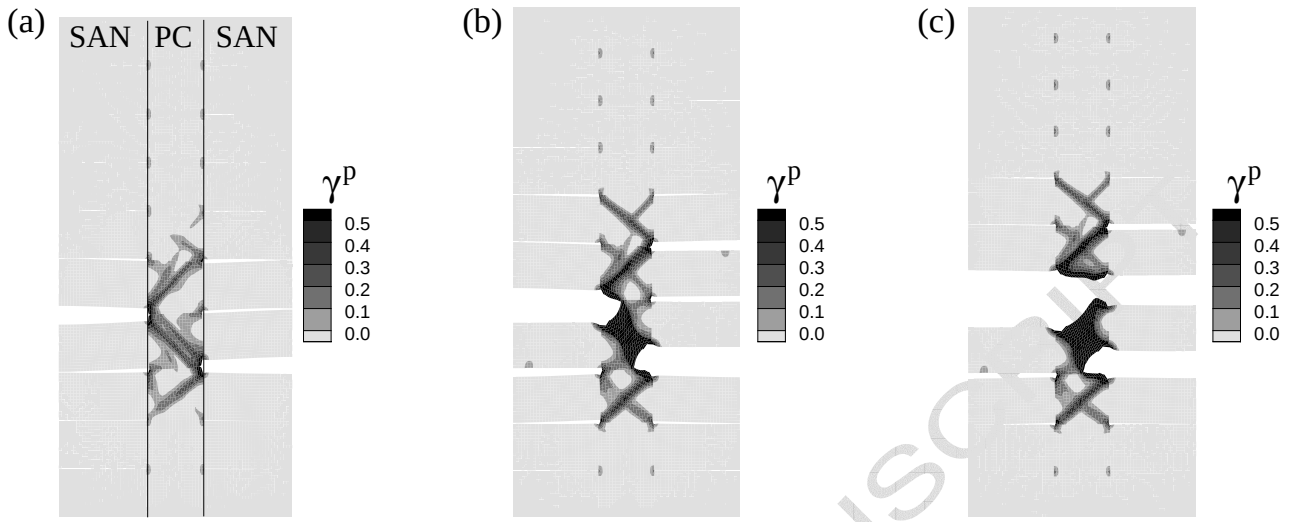

Figure 7: Contours of plastic strain γ^{p} in PC/SAN(1/3) microlayer composite at overall strain (a) $\bar{\varepsilon} = 0.056$, (b) $\bar{\varepsilon} = 0.11$, (c) $\bar{\varepsilon} = 0.14$.

dependence on the relative layer thickness, can be explained from the simple kinematical consideration sketched in Fig. 8a. Widening of a craze at a rate $\dot{\Delta}$ in one SAN layer is transferred by the shear bands in the neighboring PC layer to the next SAN layer. There an extra strain rate $\dot{\varepsilon}$ (in addition to the elastic deformation) is induced which scales reciprocally with the distance d of the SAN layers. Hence, the cooperation of crazes and shear bands leads to an interaction

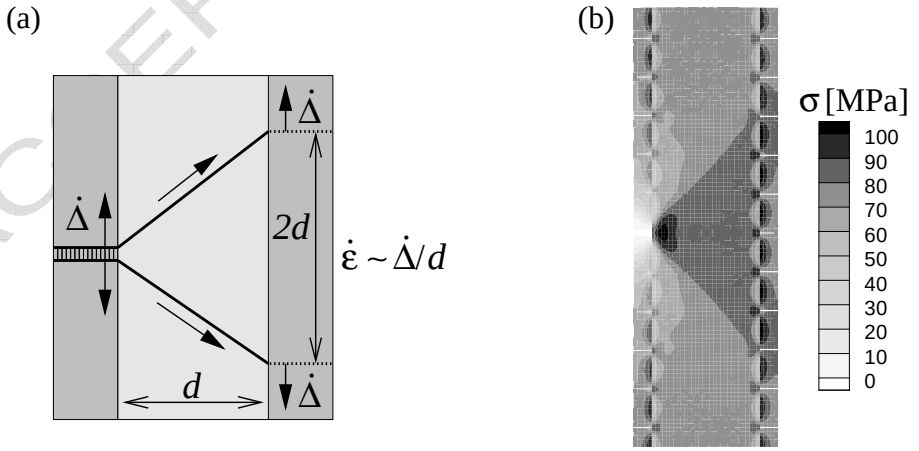

Figure 8: (a) Kinematical consideration of extra strain rate induced due to craze widening and shear banding, (b) resulting distribution of stress in vertical direction corresponding to Fig. 5a.

between neighboring SAN layers that scales nonlinearly with the layer distance. The induced stress concentration, exemplified by the contour plot of the finite element simulation in Fig. 8b that corresponds to Fig. 5a, is stronger and more localized for a smaller layer distance. This corresponds to the localized brittle failure of SAN-rich composites observed in experiments as well as in the simulations.

4.2 Distributed initial defects

In order to render the computational model more realistic, we now look at a somewhat larger sample of the composite material (consisting of two layers of each constituent) and assume the craze initiation stress on the individual cohesive zones in the SAN to fluctuate slightly (by 10 %) around the value given in Table 2. Again, a PC-rich and a SAN-rich composite are analyzed with the same relative layer thicknesses and subjected to the same loading conditions as in Sect. 4.1.

Figure 9 illustrates the situation in the PC-rich composite at two levels of overall strain. In Fig. 9a several randomly distributed crazes (or microcracks) have formed from initial defects (weaker cohesive zones). Shear bands in the PC have initiated individually from the tips of these separation zones and form a network that resembles very much the situation observed in experiments for a material with comparable composition (Fig. 1b). The distribution of stress in the loading direction (parallel to layers) at the same instant ($\bar{\varepsilon} = 0.07$) is shown in Fig. 9b. It reveals that the crazes in fact have already turned into cracks. From Fig. 9b it can also be seen that, apart from local unloading above and below the cracks and stress concentrations ahead of their tips, the overall load is relatively well balanced between the two phases – despite local fractures in the SAN! Even at 20 % overall strain (Fig. 9c) there is no indication of a localization of failure; the number of cracks in the SAN layers has increased, but they are distributed throughout the sample and connected by shear band in the PC. Those cracks which have grown to holes are more or less arranged in a diagonal pattern, and the situation visible in Fig. 9c resembles that in Fig. 1c.

From the simulation of the SAN-rich composite with the same distribution of initial defects the local scenario depicted in Fig. 10 is obtained. Similar to the situation with a single imperfection (Fig. 7) failure of the SAN layers takes place localized and does not spread in the composite; see Figs. 10a and c. The stress is then concentrated in the PC in the vicinity of the cracks (Fig. 10b) and leads to massive local plastic deformation in the PC layers so that they rupture at relatively small overall strain. Figure 10c shows the situation when both PC layers

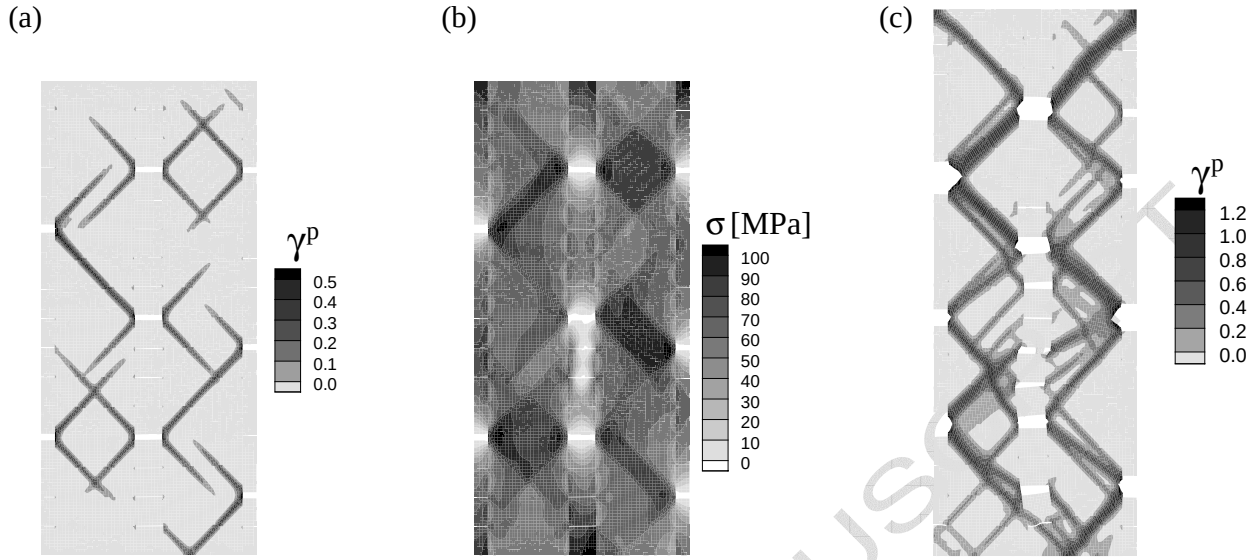

Figure 9: PC/SAN(3/1) microlayer composite with distribution of (a) plastic strain γ^{p} at overall strain $\bar{\varepsilon} = 0.07$, (b) stress in vertical (loading) direction at $\bar{\varepsilon} = 0.07$, (c) γ^{p} at $\bar{\varepsilon} = 0.2$.

of the sample have failed and the composite has effectively lost its load-carrying capacity.

Since the sample of material considered here and the number of layers is rather small compared to real specimens in the experiments, the simulations have for both composites been repeated with different distributions of initial defects in order to analyze the sensitivity of the

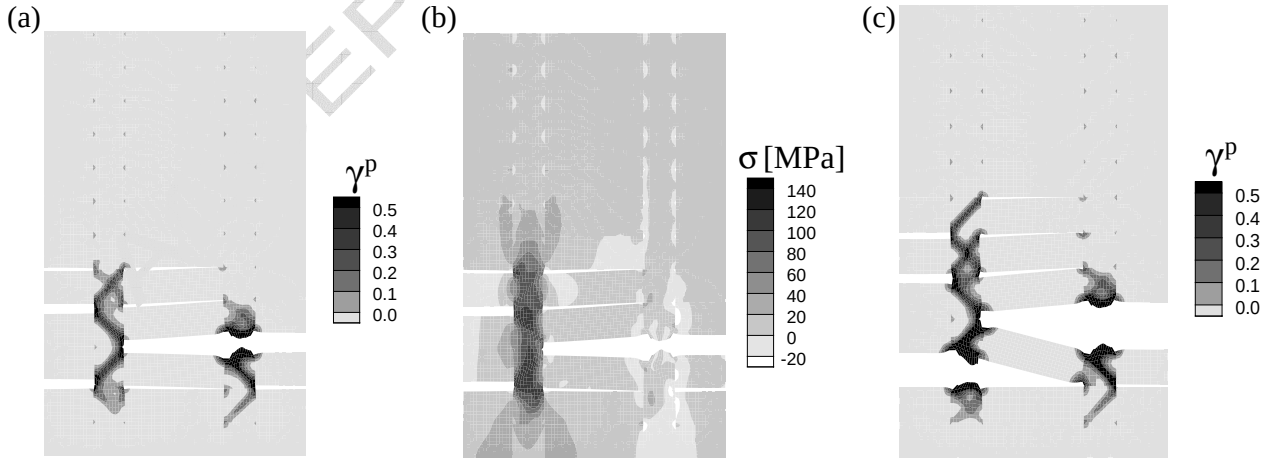

Figure 10: PC/SAN(1/3) microlayer composite with distribution of (a) plastic strain γ^{p} at overall strain $\bar{\varepsilon} = 0.05$, (b) stress in vertical (loading) direction at $\bar{\varepsilon} = 0.05$, (c) γ^{p} at $\bar{\varepsilon} = 0.09$.

numerical results with respect to this distribution. In terms of the macroscopic stress-strain response the results for PC-rich and SAN-rich composites are collectively depicted in Fig. 11 and show a good reproducability. They are in qualitative and, to some extent, also quantitative agreement with experimental findings reported by Gregory et al. (1987) and Im et al. (1991) in that SAN-rich composites fail in a brittle manner at a few percent overall strain due to the localized coalescence of microcracks (see also Fig. 1a) whereas PC-rich composites display a ductile behavior with a stress plateau somewhat below the peak load.

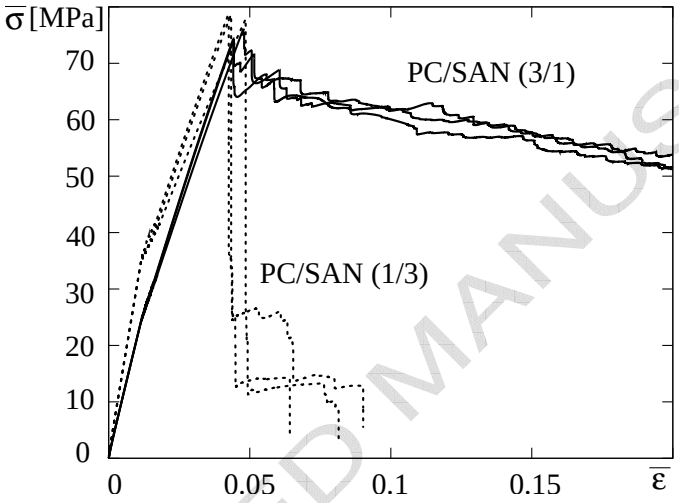

Figure 11: Macroscopic response of PC-rich (solid curves) and SAN-rich (dotted curves) composites, three simulations each with different distributions of craze initiation stress.

The numerical simulations provide additional insight into the deformation and failure processes not accessible by experiments. For instance, they allow to monitor the different energy portions, i.e. the elastically stored energy W_{el}, the plastic work W_{pl} dissipated in the bulk and the cohesive work W_{coh} consumed by separation on the cohesive surfaces, which according to the energy balance sum up to the total work W_{tot} expended to the sample by the external loading. Figure 12 shows, normalized by the total work, the variations of these energy portions in the course of overall deformation for the PC-rich (a) and the SAN-rich (b) composite. For both materials it can be seen that the elastic energy decreases as W_{coh} increases due to craze widening prior to any plastic bulk deformation. Once shear bands start to develop in the PC-rich composite (Fig. 12a) the plastic work increases rapidly, yet continuously, while the portion of cohesive work decreases. Hence, in the PC-rich composite the major part of the energy is dissipated by plastic deformation in the bulk. In the SAN-rich composite (Fig. 12b) the amount

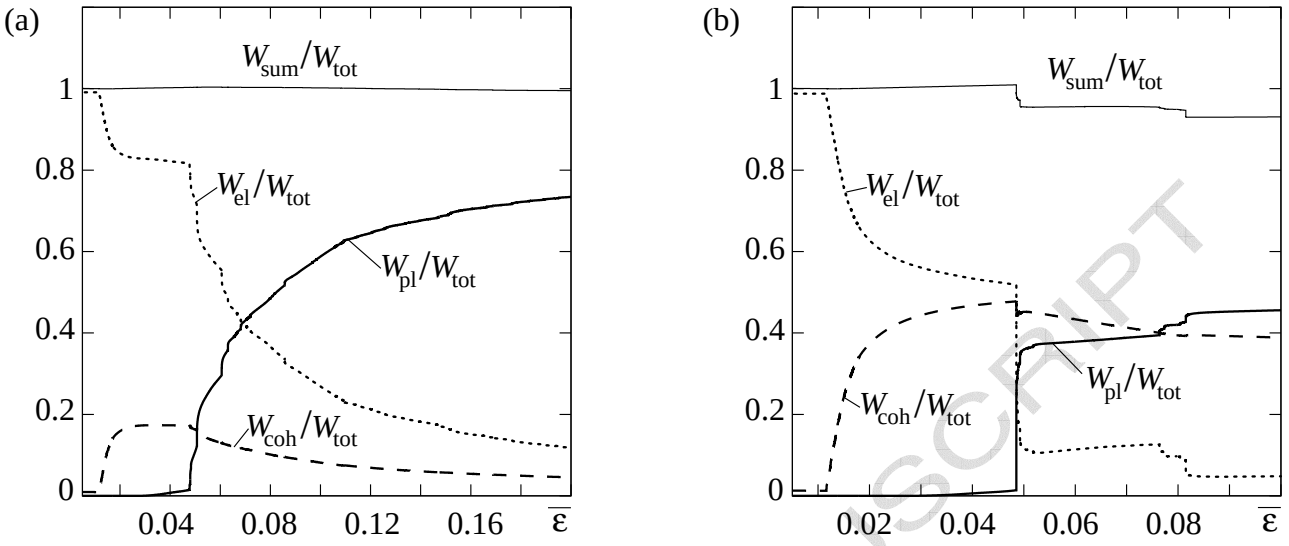

Figure 12: Energy portions normalized by total work in case of (a) PC/SAN (3/1) and (b) PC/SAN (1/3) multilayer composite.

of energy dissipation by crazing (W_{coh}) in the early stage of loading is much larger than in the PC-rich composite. When at about 5 % overall strain collective failure of the SAN layers takes place in the SAN-rich composite (see Figs. 10a and b) the load is carried solely by the PC layers and the portion of plastic work abruptly increases (Fig. 12b). At the same time a large amount of elastic energy is released (stress drop in Fig. 11) which cannot be fully absorbed by plastic dissipation. Hence, this fracture process takes place in an unstable manner and the quasi-static energy balance is violated as can be seen from the drop in the ratio $W_{\mathrm{sum}}/W_{\mathrm{tot}}$ in Fig. 12b which in equlibrium should always be equal to 1. Cohesive work by separation and plastic deformation in the bulk contribute by the same order to energy dissipation in the total fracture process in the SAN-rich composite as indicated by the approximately same level of the dashed and the thick solid curve at the final stage in Fig. 12b.

5 Discussion and conclusions

Utilizing appropriate constitutive models for the characteristic behavior of both constituents, multilayer composites of a ductile (PC) and a brittle (SAN) glassy polymer subjected to tensile loading have been investigated by numerical simulations. The simulations well reproduce the experimentally observed local and overall response of the composites which is controlled by the

relative layer thickness in conjunction with the interaction between crazes (or microcracks) and shear bands. The detailed analysis of these micromechanisms allows to better understand the transition between an overall ductile response and localized brittle failure when the distance between the SAN layers becomes smaller. In case of PC-rich composites the interaction between crazes and shear bands leads to a delocalization of damage and hampers the formation of a macroscopic crack. Although the present study which has to be understood as a first step already provides some insight into the micro- and macromechanical behavior of amorphous thermoplastic multilayer composites, some shortcomings have to be mentioned which will be the subject of future research.

So, it should be noted that the model predictions are not entirely consistent with the experiments where a successive formation and widening of new crazes in the SAN is observed in the loading regime prior to failure. This leads to a dense network of crazes and shear bands throughout large regions of the material even in SAN-rich composites visible in Fig. 1a but not in the simulations (Fig. 7 and 10). A possible reason might be the not yet proper shape of the traction-separation law. Not analyzed in the present work are the experimentally observed effects of the loading rate and the *absolute* layer thickness (Gregory et at., 1987). The latter introduces a clear size effect in the experiments for layer thicknesses below a micron. The difficulty to describe crazing in the vicinity of an interface by means of a cohesive surface (see Fig. 4) might be avoided by an alternative approach representing crazes by a continuum model as proposed in (Socrate et al., 2001) and (Challier et at., 2006).

As a final remark, it should be mentioned that the mechanism of splitting the brittle SAN layers into finite pieces connected by the intermediate ductile PC layers, giving rise to a large deformability in case of PC-rich composites (see Figs. 1c, 5c and 9c), resembles much what has recently been observed as nano-scale deformation between brittle mineral platelets and the ductile collagen matrix of bone (Gupta et al., 2006). It would therefore be interesting and challenging to apply a micromechanical model as set up in the present work to explore the above mentioned deformation mechanism in biological materials.

Acknowledgment

Financial support of this work by the German Science Foundation (DFG) under grant no. SE 872/5-1 is gratefully acknowledged.

References

Basu, S., Mahajan, D.K., Van der Giessen, E., 2005. Micromechanics of the growth of a craze fibril in glassy polymers. Polymer 46, 7504-7518.

Boyce, M.C., Parks, D.M. and Argon, A.S., 1988. Large inelastic deformation of glassy polymers. Mech. Mater. 7, 15-33.

Bucknall, C.B., 1977. Toughened Plastics. Applied Science, London.

Callier, M., Besson, J., Laiarinandrasana, L. and Piques, R., 2006. Damage and fracture of polyvinylidene flouride (PVDF) at 20°C: Experiments and modelling. Eng. Frac. Mech. 73, 79-90.

Danielsson, M., Parks, D.M. and Boyce, M., 2002. Three-dimensional micromechanical modeling of voided polymeric materials. J. Mech. Phys. Solids 50, 351-379.

Estevez, R., Tijssens, M.G.A. and Van der Giessen, E., 2000. Modeling the competition between shear yielding and crazing in glassy polymers. J. Mech. Phys. Solids 48, 2582-2617.

Estevez, R. and Van der Giessen, E., 2005. Modeling and Computational Analysis of Fracture of Glassy Polymers. Adv. Pol. Sci. 188, 195-234.

Gregory, B.L., Siegmann, A., Im, J., Hiltner, A., Baer, E., 1987. Deformation behaviour of coextruded multilayer composites with polycarbonate and poly(styrene-acrylonitrile). J. Mat. Sci. 22, 532-538.

Gupta, H.S, Seto, J., Wagenmaier, W., Zaslansky, P., Boesecke, P., Fratzl, P., 2006. Cooperative deformation of mineral and collagen in bone at the nanoscale. PNAS 103, 17741-17746.

Haward, R.N. and Young, R.J., 1997. The Physics of Glassy Polymers. Chapman & Hall.

Im, J., Baer, E. and Hiltner, A., 1991. Microlayer Composites, in: Baer, E. and Moet, A. (Eds.) High Performance Polymers, 175-198, Hanser Publishers

Kerns, J., Hsieh, A., Hiltner, A. and Baer, E., 2000. Comparison of irreversible deformation and yielding in microlayers of polycarbonate with poly(methylmethacrylate) and poly(styrene-co-acrylonitrile). J. Appl. Pol. Sci. 77, 1545-1557.

Kinloch, A.J. and Young, R.J., 1983. Fracture Behaviour of Polymers. Applied Science Pub-

lishers.

Lauterwasser, B.D. and Kramer, E.J., 1979. Microscopic mechanisms and mechanics of craze growth and fracture. Phil. Mag. A 39, 469-495.

Martuscelli, E. (Ed.), 1996. Advanced routes for polymer toughening. Elsevier.

Meijer, H.E.H. and Govaert, L.E., 2003. Multi-scale analysis of mechanical properties of polymer systems. Macromol. Chem. Phys. 204, 274-288.

Narisawa, I. and Yee, A.F., 1993. Crazing and Fracture of Polymers. In: Structure and Properies of Polymers; Material Science and Technology, A Comprehensive Treatment, Vol. 12. VCH, 698-765.

Pijnenburg, K.G.W., Steenbrink, A.C. and Van der Giessen, E., 1999. Shearing of particles during crack growth in polymer blends. Polymer 40, 5761-5771.

Saad-Gouider, N., Estevez, R., Olagnon, C. and Seguela, R., 2006. Calibration of a viscoplastic cohesive zone for crazing in PMMA. Engng. Fract. Mech. 73, 2503-2522.

Seitz, J.T., 1993. The estimation of mechanical properties of polymers from molecular structure. J. Appl. Pol. Sci. 49, 1331-1351.

Socrate, S., Boyce, M.C. and Lazzeri, A., 2001. A micromechanical model for multiple crazing in high impact polystyrene. Mech. Mater. 33, 155-175.

Sung, K., Hiltner, A. and Baer, E., 1994. Three-dimensional interaction of crazes and microshearbands in PC-SAN microlayer composites. J. Mat. Sci. 29, 5559-5568.

Tijssens, M.G.A., Van der Giessen, E. and Sluys, L.J., 2000. Modeling of crazing using a cohesive surface methodolgy. Mech. Mater. 32, 19-35.

Tomita, Y., 2000. Constitutive modelling of deformation behavior of glassy polymers and applications. Int. J. Mech. Sci. 42, 1455-1469.

Van der Giessen, E., 1997. Localized plastic deformations in glassy polymers. Eur. J. Mech., A/Solids 16, 87-106.

Wu, P.D. and Van der Giessen, E., 1996. Computational aspects of localized deformations in amorphous glassy polymers. Eur. J. Mech. A/Solids 15, 799-823.

List of Figures